Numerical Simulation of Dendrite Growth during Solidification

X. Yao[1, 2], H. Wang[1], B. He[2] and X. Zhou[2]

[1]School of Engineering, The University of Queensland, St Lucia, QLD 4072, Australia
[2]School of Mechanical and Electrical Engineering, East China Jiaotong University, Jiangxi, China

ABSTRACT

A comprehensive probabilistic model for simulating dendrite morphology and investigating dendritic growth kinetics during solidification has been developed, based on a modified Cellular Automaton (mCA) for microscopic modeling of nucleation, growth of crystals and solute diffusion. The mCA model numerically calculated solute redistribution both in the solid and liquid phases, the curvature of dendrite tips and the growth anisotropy. This modeling takes account of thermal, curvature and solute diffusion effects. Therefore, it can simulate microstructure formation both on the scale of grain size and dendrite tip length. This model was then applied for simulating dendritic solidification of an Al-7%Si alloy. Both directional and equiaxed dendritic growth has been performed to investigate the effect of growth anisotropy and cooling rate on dendrite morphology. Furthermore, competitive growth and selection of the dendritic crystals have also been investigated.

INTRODUCTION

The Cellular Automaton (CA) technique[1] has successfully applied to generate realistic-looking microstructures as it is based on the consideration of physical mechanisms of nucleation, growth kinetics and crystallographic orientation competition. However, the original CA is only related to local temperature in the solidifying area for a given alloy composition, which implies that only the thermal effect is considered in the CA model. Therefore, it is unable to describe the detail dendritic features such as the side branches, which are controlled by solute redistribution and curvature effect.

Phase field models[2, 3] offer an opportunity for predicting dendritic growth with a description of detail features of dendrites and a better understanding of dynamics of dendritic pattern selection, however, phase field models are limited to calculate just a few dendrites within a small domain due to the large computational capacity needed. There exists a length-scale gap between the CA model and the phase field models in predicting microstructure formation .

The CA algorithm has been modified by Nastac[4], Zhu and Hong[5] and Yao et al[6], which incorporates the effects of solute redistribution and dendrite tip capillarity into the model in order to simulate the concentration field and dendrite morphology on a mesoscopic level. The modified model takes account of thermal, solute and capillary effects into nucleation and growth, to simulate the dendritic microstructure formation in a much bigger domain compared with the phase field method and the interactions of dendritic grains during solidification. However, it should be noted that this method is also limited to a small domain compared with the original CA algorithm due to a much finer mesh is required for the solute field calculation.

MODEL DESCRIPTION

The governing equations

Neglecting the effect of convection, the solidification process is controlled by thermal and solute diffusion. The equations that describe the physics of these processes are:

- Thermal diffusion: Assuming that the whole domain is in a uniform temperature and cools with a constant cooling rate, $\dot{a}$, for equiaxed solidification.

$$\frac{\partial T}{\partial t} = -\dot{a} + \frac{L}{\rho c_p}\frac{\partial f_S}{\partial t} \quad (1)$$

where T is temperature, t is time, ρ is the density, c_p is the specific heat and L is the latent heat.

- Solute diffusion and curvature have been treated as described by Nastac[4], where diffusion in a dilute binary system is given by:

$$\frac{\partial C_i}{\partial t} = \nabla(D_i \nabla C_i) \quad (2)$$

where D is the interdiffusion coefficient, $i = L,\ S$ represent the liquid and solid phase respectively.

- The average interface for a cell with the solid fraction, f_S, is calculated with the following equation[5]:

$$\overline{K} = \frac{1}{a}[1 - 2\frac{f_S + \sum_{i=1}^{N} f_s(i)}{N+1}] \quad (3)$$

where N is the number of the neighbouring cells. In the present calculations, N=8, that includes the first order neighbouring cells. The values of curvature calculated by equation (3) vary from a maximum $1/a$ to zero for a convex surface and zero to $-1/a$ for a concave surface.

- Local equilibrium at the solid/liquid interface ("*" means at the interface):

$$C_S^* = kC_L^* \quad (4)$$

where k is the partition coefficient. The effective partition coefficient in rapid solidification is derived by Aziz et al.[7]

Nucleation Module

Same as for previous algorithms, a continuous nucleation model with Gaussian distribution was used to describe the grain density increase, *dn*, which is induced by an increase in the undercooling, $d(\Delta T)$. Then the total density of grains, $n(\Delta T)$, which has been nucleated at a given undercooling, ΔT, is given by

$$n(\Delta T) = \int_0^{\Delta T} \frac{dn}{d(\Delta T)} d(\Delta T) \quad (5)$$

Growth Module

If the kinetics and curvature contributions of undercooling are neglected, the local undercooling at time *t*, $\Delta T(t)$, can be given by

$$\Delta T(t) = T^{EQ} - T(t) = T_L + m_L(C(t) - C_0) - T(t) \quad (6)$$

where T^{EQ} is the local equilibrium liquidus temperature at a local composition *C(t)* in the liquid, T_L is the equilibrium liquidus temperature with concentration C_0, m_L is the slope of liquidus and C_0 is the initial concentration of the alloy. Then, the growth velocity, $V^*(t)$, can be calculated using models such as the KGT model[8] with the interface undercooling.

For directional solidification with a given thermal undercooling, *G*, a barrier is being established by solute build-up that retards the velocity by $V_b(t)$[9].

$$V_b(t) = -\frac{m_L}{G}\frac{dC_L^*}{dt} \quad (7)$$

Therefore, the interface growth velocity for directional solidification, $V_i(t)$, is given by

$$V_i(t) = V(t) - V_b(t) \quad (8)$$

As in previous models, the growth length of the dendrite tip, $L(t)$, during one time step, δt, is given by

$$L(t) = \frac{V_i(t) \cdot \delta t}{(\cos\theta + |\sin\theta|)} \quad (9)$$

where θ is the angle of the preferential growth direction with respect to the horizontal direction of the cell. When $L(t)$ is greater than the length of the CA cell, which means that the growing dendrite tip from a solid cell touches the centre of its neighboring liquid cell, the entrapment of the nearest-neighboring cell occurs, and the dendrite in this cell grows in the same direction.

RESULTS AND DISCUSSION

In the present work, the dendritic growth of an Al-Si alloy is studied and the calculations are performed in two stages. Firstly, calculations are performed within a $300\mu m$ x $300\mu m$ domain to investigate the equiaxed dendritic growth. Then they are performed within a $300\mu m$ x $1000\mu m$ domain to investigate the directional dendritic growth. The domain is small enough to be considered as a uniform temperature. Thermophysical properties of the alloy used for simulation are given in Table 1.

Table 1 Thermophysical properties of Al-Si alloys[10]

T_m^{Al} (K)	T_{eut} (K)	C_{eut} (wt%)	k_0 (-)	m_L (°C/%)	ΔH_V (J/m^3)
933	850	10.77	0.117	6.5	1.107×10^9
ρ (kg /m^3)	C_p (J/kg K)	λ (W/m K)	D_l (m^2/s)	D_s (m^2/s)	Γ (K m)
2720	1086	192.5	3×10^{-9}	1×10^{-12}	0.9×10^{-7}

Free Dendritic Growth

Figure 1 shows the formation and evolution of dendrite morphology and solute pattern in Al-7%Si alloy predicted by the proposed mCA model using different crystallographic orientations, 20° and 48°, respectively. The solidification follows the procedure of initial growth before marginal instability of dendrite, initiation of secondary arms, and growth to a well-developed dendrite with secondary and tertiary branches. Coarsening of secondary and tertiary arms is also observed. The final dendrite morphology is very different for the different growth anisotropy. The dendrite with 20° exhibits a spherical geometry without obvious first arms, however, the dendrite with 48° exhibits near-square morphology with obvious first arms. Figure 2 shows the impingement of the solute fields and the physical dendrites for the alloy. The impingement of the solute fields is earlier than the impingement of the physical dendrites. When the solute layers around dendrites meet, the growth velocity of dendrites decreases to a very low value by suppression of the solute[6] and then, the growth of the dendrite arms in this area is largely restrained. The growth of dendrites in the other areas continues, forming a dendrite with well-developed secondary and tertiary branches. Figure 3 shows the effect of cooling rate on dendrite formation during solidification. A high cooling rate results a more well-developed solidified dendrite than a low cooling rate. Figure 4 shows that when a dendrite grows with a relatively high velocity, the dendrite tip may break through the solute layer and grow into the undercooled liquid region because the thickness of solute layer in front of the dendrite tip is very small in rapid growth and the morphology of the dendrite tip is very sharp due to large enrichment of the solute. Then, the growth of the dendrite tip is in a very high velocity duo to the large undercooling in the constitutional undercooled zone. The dendrite reaches the whole domain very quickly. It is demonstrated from these results that the proposed model is very successful in depicting the evolution of dendritic features during solidification, including the growing and coarsening of primary arms, the branching of secondary and tertiary dendrite arms, and the solute concentration pattern.

Directionally Solidified Dendrite Morphology Formation

Figure 5 shows the morphology formation and evolution of dendrites for an Al-7%Si alloy with crystallographic orientations of 0° and 20° corresponding to the direction of the heat flow. The solute pattern ahead of the growing front is also shown. With the orientation of 0°, the primary trunk of the dendrite is in <001> direction which is parallel to the direction of heat flow. This leads that the primary trunk will grow much faster than the other branches. The primary arm spacing can be easily adjust to a unique value corresponded to the given growth velocity, and the growth is easier to reach a steady state. While with the orientation of 20°, the <001> direction of the dendriteis also deviated from the direction of heat flow with 20°. When the dendrite grows, the branches of the crystals, which have a less deviation with the heat flow direction will grow faster than the others, and become the primary arms. The average primary arm spacing of the final microstructure is much smaller than that of the orientation 0°. The secondary and tertiary arms are well developed in both dendrite growth, but the dendrite with orientation 0° exhibits a more regular microstructure. Figure 6 shows the growth competition of dendrite crystals during dendritic solidification. Many dendrites initially form at mould wall then grow opposite the direction of the heat flow. Dendrites with a deviation from the direction of heat flow grow slower and the dendrite tips/liquid interfaces are in a back position. Simultaneously, the rejected solute from the faster growing dendrite forms a solute enrichment area in the front of the behind dendrites. According to the growth dynamics of alloy solidification, the growth rate within high concentration is lower than that within low concentrations. Thus, the growth rate of the behind dendrites is further decreased and the growth of those dendrites is depressed. This results in the elimination of those dendrites in a competed growth. The branching of the advanced growing dendrite is also an important factor to adjust the primary arm spacing by depressing the growth of other dendrites.

CONCLUSIONS

A modified CA model for simulating microstructure formation has been developed. This model takes account of the effects of solute redistribution, curvature and growth anisotropy. A new growth model based on the analysis of the role of solute redistribution on the growth kinetics was proposed.

The crystallographic orientation of a nucleus has significant effect on the dendrite morphology and dendritic arm spacing. The solute fields of crystals impinged before the physical impingement. At the impingement of solute field, the growth rate of crystals decreases greatly then dendrites become mainly coarsening. The dendrite tip with high solute enrichment around solidifying undercooling a relatively high cooling rate could penetrate through the solute layer and grows into the undercooled zone and then, grows very fast. However, the simulated morphology has not been observed in experimental investigations. The crystallographic orientation of the wall crystals has also a significant effect on dendritic array selection and dendrite arm spacing during directional dendritic solidification. Competitive growth of dendrites leads to dendrite arm spacing selection.

REFERENCES

1. M. Rappaz and Ch.-A. Gandin, “Probabilistic Modelling of Microstructure Formation in Solidification Processes”, *Acta Metall.*, **41**, 345(1993).
2. W. J. Boettinger, J. A. Warren, C. Bechermann and A. Karma, *Annual Rev. of Mater. Res.*, **32**, 163(2002).
3. A. Karma and W. J. Rappel, *Physical Review E*, **57**, 4323(1998).
4. L. Nastac, *Acta Mater*. **47**, 4253(1999).
5. M. F. Zhu and C. P. Hong, *ISIJ Int*. **41**, 436(2001).
6. X. Yao, C. J. Davidson, A. K. Dahle and D. H. StJohn, *Int. J. Cast Metals Res*. **15**, 219(2003).
7. M. J. Aziz, *J. Appl. Phys.*, **53**, 1158(1982).
8. W. Kurz, B. Giovanola and R. Trivedi, *Acta Metall.*, **34**, 823(1986).
9. W. D. Huang, Q. M. Wei and Y. H. Zhou, *J. Crystal Growth* **100**, 26(1990).
10. W. Kurz and D. J. Fisher, *Fundamental of Solidification*, Trans Tech Publications, Aedermannsdorf, Switzerland, (1989), pp.240.

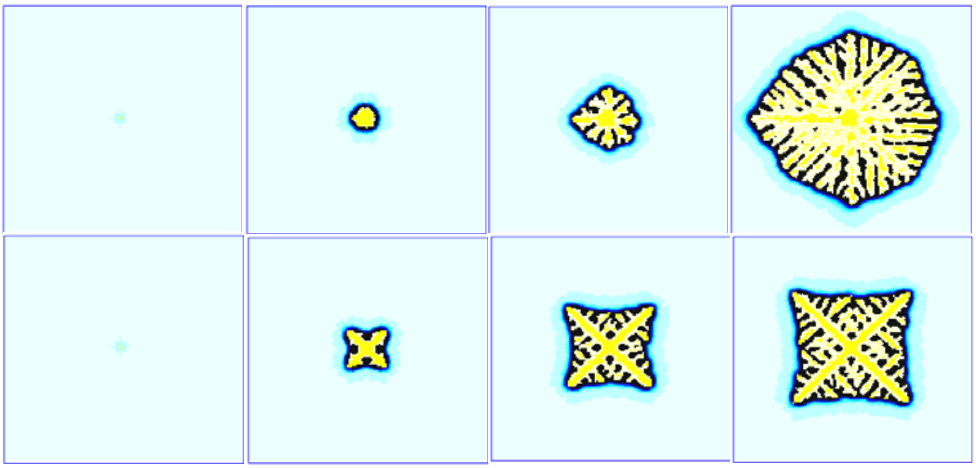

Figure 1. Prediction of dendrite morphology at a cooling rate 0.02K/s for a given nucleus (a) Orientation=20^0, t=0.1, 0.3, 0.5, 0.97s (b) Orientation=48^0, t=0.1, 0.3, 0.5, 0.63s

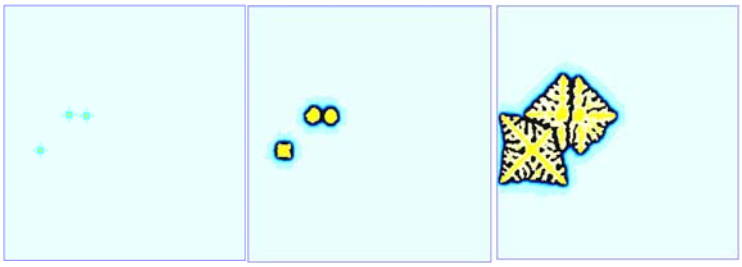

Figure 2. Impingement of dendrites during solidification, t=0.2, 0.4, 0.7s
Nucleation site density in the melt, $n_v = 5.2 \times 10^9$, cooling rate=0.02 K/s

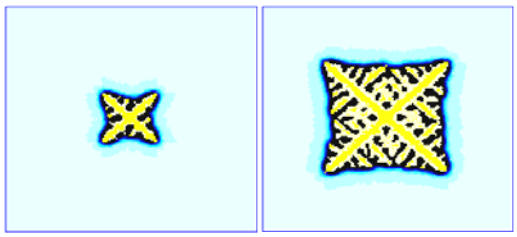

Figure 3. Effect of cooling rate on equiaxed dendrite growth for a given nucleus, t=0.63s, (a) 0.02 K/s (b) 0.2 K/s

Figure 4. Growth of dendrite tip into undercooled melt through solute layer with a cooling rate 2 K/s for a given nucleus, t=0.34, 0.36, 0.364s

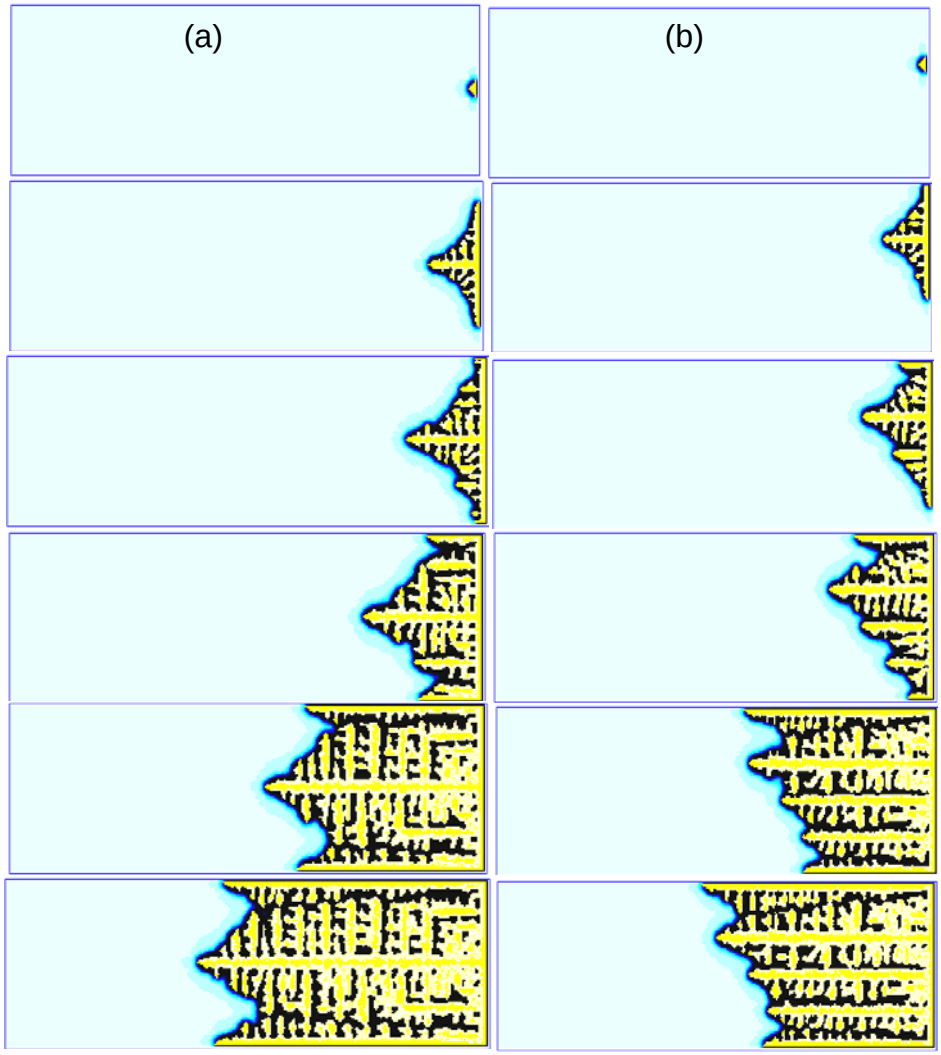

Figure 5. Dendrite morphology formation and evolution with time at a cooling rate 0.02 K/s for a given nucleus (a) Orientation=0^0, N=100, 800, 1200, 1800,3200,4083 (b) Orientation=20^0, t=0.1, 0.8, 1.2, 1.8, 3.2, 3.7s

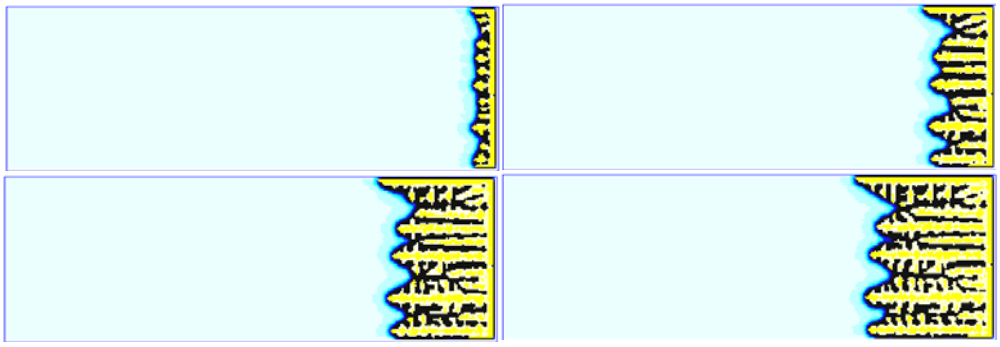

Figure 6. Dendrite morphology formation and evolution with time at a cooling rate 0.02K/S, t=0.5, 1.25, 1.75, 2s, Nucleation site density at the wall, $n_s = 2.5 \times 10^8$